Mass dependence of pion double charge exchange

R. Gilman,* H. T. Fortune, J. D. Zumbro, and C. M. Laymon
University of Pennsylvania, Philadelphia, Pennsylvania 19104

G. R. Burleson, J. A. Faucett, and W. B. Cottingame†
New Mexico State University, Las Cruces, New Mexico 88003

C. L. Morris
Los Alamos National Laboratory, Los Alamos, New Mexico 87545

Peter A. Seidl,‡ C. Fred Moore, L. C. Bland,§ and Rex R. Kiziah**
University of Texas at Austin, Austin, Texas 78712

S. Mordechai††
University of Pennsylvania, Philadelphia, Pennsylvania 19104
and University of Texas at Austin, Austin, Texas 78712

Kalvir S. Dhuga‡‡
University of Pennsylvania, Philadelphia, Pennsylvania 19104
and New Mexico State University, Las Cruces, New Mexico 88003
(Received 18 August 1986)

Data are presented for pion double charge exchange on targets of ^{44}Ca, ^{56}Fe, ^{58}Ni, ^{80}Se, ^{90}Zr, and ^{118}Sn. These and earlier data are used to examine the mass dependence of double-isobaric-analog transitions and nonanalog ground-state-to-ground-state transitions in the energy region $T_\pi = 100$ to 300 MeV. The implications of the mass dependence to the interpretations of the underlying reaction mechanisms of double charge exchange are discussed.

I. INTRODUCTION

The mass dependence of pion double charge exchange (DCX) has been a topic that has evoked much discussion. Prior to any experimental evidence, Johnson[1] derived the mass dependence of sequential charge exchange leading to double-isobaric-analog states (DIAS's) as

$$\frac{d\sigma}{d\Omega}(q=0) \propto (N-Z)(N-Z-1)A^{-10/3} .$$

Several subsequent articles comparing data (typically at $\theta_{\rm lab}=5°$) with the above expression have appeared.[2–6] Most of these made a graphical comparison of the data to this expected mass dependence and concluded that there is good agreement. One of them noted,[6] however, that if only $T=1$ nuclei are considered, the A dependence is closer to $A^{-7/3}$ than $A^{-10/3}$.

The agreement has been observed to be better at the higher energies (292 MeV) than at the lower energies (164 MeV). This arises from the variation in the shapes of the excitation function of the DIAS transitions. Above about 180 MeV, all DIAS excitation functions increase monotonically at about the same rate (the explanation can be seen from the equations of Ref. 1). Below this energy, the behavior of the excitation functions is different for different nuclei. The ^{14}C excitation function, for example, is roughly flat from 100 to 140 MeV, and increases monotonically above this energy, whereas the ^{18}O excitation function has a peak at about 140 MeV and a minimum at about 180 MeV. As a result, the graphical mass-dependence comparisons at lower energies (164 MeV) have shown much scatter among the data.

Until recently,[7] there has been no satisfactory microscopic theory of the non-DIAS DCX transitions connecting initial 0^+ ground states to residual nonanalog 0^+ ground states. These transitions have been shown to exhibit regular features[8,9]—in particular, a mass dependence that has usually been approximated as $\sigma \sim A^{-4/3}$. (We note that we use the term "mass dependence" to refer to the combined N, Z, and A dependences.) This results from a comparison of forward-angle cross sections, which, while lacking theoretical justification, is the only practical manner in which such comparisons may be made. The long data-taking times required to measure nonanalog DCX cross sections have resulted in only a small number of angular distributions (six), which are limited in angular range (0°–50°), and thus inappropriate for an attempt to compare total cross sections.

The forward-angle result is both very different from that of DIAS DCX, and unexpected. It has usually been assumed that both nonanalog and DIAS DCX result from sequential single-charge exchange. Two-step DCX processes are generally expected to have an $A^{-10/3}$ mass dependence (although we know of no formal derivations that do not assume intermediate and residual analog states). The exponent $-\frac{10}{3}$ comes from a geometrical size

of $r^2 \propto A^{2/3}$ and the two-step reaction, with the amplitude of each step being proportional to $1/A$. In a crude model, the volume of the nucleus is proportional to A; thus a nucleon's wave function must be proportional to $A^{-1/2}$. The amplitude for each step is then $1/A$ since this is the probability of finding a nucleon at some position in the nucleus. This crude argument holds as well for diagrams other than sequential charge exchange. There are however, no good arguments about what, if any, N and Z dependence are appropriate for nonanalog DCX.

In this paper we present some additional measurements of DCX cross sections. A comprehensive statistical analysis of both analog and nonanalog mass dependences is presented for all data at energies between 100 and 300 MeV (some earlier works have reported best-fit exponents). A comparison is made of DIAS cross sections with calculations. Finally, we discuss the implications of the mass dependence for interpretations of the underlying reaction mechanism.

II. NEW EXPERIMENTAL RESULTS

The experimental measurements were performed with the small-angle DCX setup at the EPICS channel of the Clinton P. Anderson Meson Physics Facility (LAMPF). Descriptions of DCX experimental procedures have appeared in the literature (see, e.g., Refs. 2–6, 8, and 9). Targets used included ^{44}Ca (0.86 g/cm^2 as $^{44}CaCO_3$ powder packed in thin-walled nickel cells) ^{56}Fe (2.44 g/cm^2 of ^{nat}Fe), ^{58}Ni (2.46 g/cm^2 of ^{nat}Ni), ^{80}Se (1.93 g/cm^2 of ^{nat}Se powder packed in nickel cells), ^{90} Zr (0.90 g/cm^2 of isotopic metal), and ^{118}Sn (0.55 g/cm^2 of isotopic metal).

A simple spectrum is shown in Fig. 1. The measured cross sections are listed in Table I. We estimate the uncertainty in our absolute normalization to be ±10%. The ^{56}Fe data complete the excitation function of Ref. 4. A ^{80}Se excitation function was measured to investigate the variation in nonanalog excitation function shapes with mass. The use of strip targets[6] enabled simultaneous measurements of cross sections for ^{44}Ca, ^{90}Zr, and ^{118}Sn. (The slightly different energies quoted in Table I result from the different target thicknesses and the correlation of the ±1% beam momentum spread with target position.)

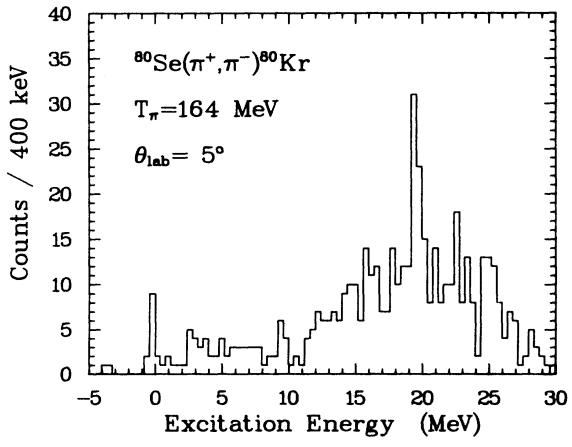

FIG. 1. Spectrum of the (π^+,π^-) reaction on a natural Se target. Much of the background arises from other Se isotopes, but the peak corresponding to ^{80}Se(π^+,π^-)^{80} Kr(g.s.) is apparent. The large peak near an excitation energy of 19.2 MeV contains the DIAS from several Se isotopes.

TABLE I. Measurements in this work.

Reaction	T_π (MeV)	$d\sigma/d\Omega_{lab}(5°)$ (nb/sr)
^{44}Ca(π^+,π^-)^{44}Ti(g.s.)	163	151±34
	210	34±20
^{44}Ca(π^+,π^-)^{44}Ti(DIAS)	163	181±42
	210	314±62
^{56}Fe(π^-,π^+)^{56}Cr(g.s.)	164	38±38
^{56}Fe(π^+,π^-)^{56}Ni(g.s.)	100	<5
	120	60±15
	180	18±5
	230	<8
	292	<11
^{56}Fe(π^+,π^-)^{56}Ni(DIAS)	100	35±26
	120	62±35
	180	41±12
	230	110±39
	292	290±68
^{58}Ni(π^-,π^+)^{58}Fe(g.s.)	164	25±18
^{80}Se(π^+,π^-)^{80}Kr(g.s.)	100	70±50
	130	120±35
	164	60±14
	190	54±31
^{90}Zr(π^+,π^-)^{90}Mo(g.s.)	164	32±23
	211	34±34
^{90}Zr(π^+,π^-)^{90}Mo(DIAS)	164	240±89
	211	209±89
^{118}Sn(π^+,π^-)^{118}Te(g.s.)	165	37±37
	212	120±84
^{118}Sn(π^+,π^-)^{118}Te(DIAS)	165	<118
	212	350±157

The ^{56}Fe and ^{80}Se excitation functions are shown in Fig. 2. The new DIAS data confirm the earlier observation[6] that the ^{56}Fe DIAS excitation function is approximately flat between ~100 and ~180 MeV. The ^{56}Fe excitation function to the residual nonanalog ground state suffers from inadequate statistics; many of the cross sections for both this and the earlier work[4] are either upper limits or one-count measurements. Although ground-state excitation functions on lighter nuclei[8] peak near 160 or 170 MeV, the peak in the ^{56}Ni (g.s.) data is nearer 140 MeV. The ^{80}Se data also appear more consistent with a peaking at a lower energy. We know of no explanation for the shift of the excitation function peak with target mass. The mass dependence is not removed by consideration of various kinematic quantities, such as the Q value, laboratory to center-of-mass conversion, or outgoing π^- energy.

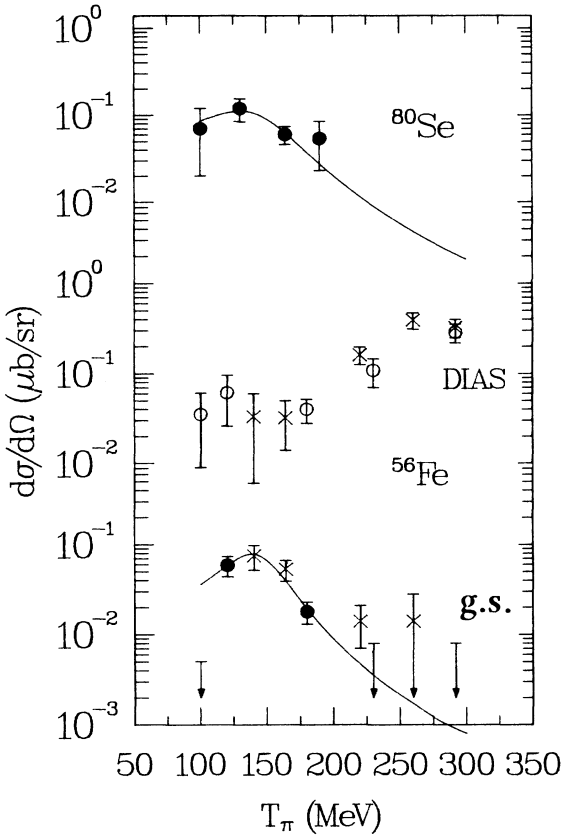

FIG. 2. Excitation functions at $\theta_{lab}=5°$ for (π^+,π^-) DCX on ^{56}Fe and ^{80}Se. Data from Ref. 4 are designated by crosses; all other data are from this work. The lines are Breit-Wigner fits to the data with the parameters of Table II. The use of the Breit-Wigner parametrization is based on the results of Ref. 8.

III. FITS TO THE DATA

The nonanalog excitation-function shapes are well parametrized with a Breit-Wigner function.[8] Results of fits to old data and the new ^{56}Fe and ^{80}Se excitation functions are displayed in Table II. [All fitting procedures reported in this work have been performed with the MINUIT (Ref. 10) optimizing package, and all reported χ^2 are the χ^2 per degree of freedom, the reduced χ^2.] The peak widths are all consistent with having a constant value, $\Gamma=74.3\pm4.7$ MeV. The peak energies are consistent with a decrease with target mass, except for the peak energy for ^{24}Mg, for which T_0 is lower than those of nearby nuclei, as has been noted before.[8] The large number of upper limits and one-count measurements in the ^{56} Fe excitation function (four of nine points) results in a fit with a very small width parameter. As a result, the table presents a fit to only the five data with more than one count.

For both nonanalog and DIAS DCX, we have simultaneously fitted the mass dependence of the center-of-mass cross sections taken at $\theta_{lab}=5°$ for several incident beam energies. A summary of the data that were fitted is given in Table III. About 20% of these data are from the present work. To emphasize the large amount of nonanalog data that has been measured, we present in Fig. 3 a comparison between these data at several energies and the often-used $A^{-4/3}$ mass dependence. In this figure it is seen that a large number of data points span a wide range of masses, and that the data appear generally well represented by the $A^{-4/3}$ expression.

We have fitted both the nonanalog and DIAS data with three different mass-dependence functions, $(N-Z)(N-Z-1)A^{-x}$, A^{-x}, and $N(N-1)A^{-x}$. The function $(N-Z)(N-Z-1)A^{-x}$, with $x=\frac{10}{3}$, represents the expected form of the DIAS mass dependence. The $(N-Z)(N-Z-1)$ factor for DIAS DCX arises from sequential charge exchange through the intermediate analog state. This factor must be inappropriate for analog DCX, as it would result in zero cross section for $N=Z$ targets, which form the bulk of the nonanalog DCX measurements. (Cross sections on these targets at 164 MeV are typically about as large as DIAS cross sections on $T=1$ nuclei of similar mass at 164 MeV.)

The function A^{-x}, with $x=\frac{4}{3}$, has been used previously[2,8] to describe nonanalog DCX. The $N(N-1)A^{-x}$ mass dependence, with $x=\frac{10}{3}$, represents a collective enhancement in the cross sections over the expected $A^{-10/3}$, since the cross section is proportional to the total number of neutron pairs (rather than to the number of excess neutron pairs to which we expect DIAS DCX to be sensitive). For each function, we have allowed the overall magnitude of the mass dependence to vary independently at each energy, but have constrained the exponent to be the same for all energies.

The results of these fits are given in Table IV. For the

TABLE II. Fitted parameters for nonanalog $0^+\rightarrow0^+$ g.s.$\rightarrow$g.s. excitation functions.[a]

Target	Reduced χ^2	g	T_0 (MeV)	Γ (MeV)
^{12}C	1.15	0.123±0.023	173.8±3.3	70.5±8.1
^{16}O	1.84	0.116±0.018	165.4±2.9	76.5±7.6
^{18}O(π^-,π^+)	0.35	0.188±0.077	174.9±6.9	84.8±22.2
^{24}Mg	2.93	0.057±0.022	143.1±5.3	65.5±16.2
^{28}Si	0.25	0.076±0.031	173.1±7.3	86.7±20.2
^{32}S	1.30	0.049±0.027	161.5±7.3	83.2±26.9
^{40}Ca	0.52	0.054±0.025	163.9±6.9	89.4±24.8
^{56}Fe	1.32	0.009±0.005	142.2±6.3	55.1±22.9
^{80}Se	0.89	0.027±0.028	139.2±9.1	82.4±50.9

[a] $(d\sigma/d\Omega)(\mu b/sr)=g\times10^4(\hbar c)^2/p^2[(T-T_0)^2+\Gamma^2/4]$, where p, T_0, and Γ are in MeV.

TABLE III. Summary of A-dependence data fitted.[a]

Type	T_π	Number of points	Average statistical error (%)
Nonanalog	120	8	23.1
	130	4	46.7
	140	9	23.1
	164	18	32.2
	180	15	35.0
	210	11	38.6
DIAS	100	4	36.2
	120	6	27.7
	140	6	29.8
	164	10	33.3
	180	10	24.9
	211	5	28.5
	230/235	8	20.1
	260	4	16.5
	292	14	16.1

[a]Data are from the present work and Refs. 2–6, 8, 9, 17, and 18.

nonanalog data, the $N(N-1)A^{-x}$ and A^{-x} formulas result in comparably good fits, as we might expect. For the large fraction of the nonanalog data that has been measured on $N=Z$ targets, these two dependences are indistinguishable (given the experimental uncertainties). We will discuss only A^{-x} fits to the nonanalog data hereafter. [We remind the reader that the $N(N-1)A^{-x}$ fit is theoretically preferable, since $x \sim \frac{10}{3}$.] A reduced χ^2 value of 2.3 for the A^{-x} dependence may indicate that this is an inadequate representation of the data. We return to this point below.

In Table V we present fits to the nonanalog data done independently at each energy with the A^{-x} function, and fits of two energy-independent parameters. The quantity g is the magnitude parameter of the fits to the nonanalog excitation functions that are given in Table II. The quantity $\sigma(T_0)$ is the fitted cross section of the nonanalog excitation functions at the peak energy. Although most of the resulting fits have χ^2 near 1.0, only about half of the fits have exponents consistent with $-\frac{4}{3}$. There appears to be some energy dependence to the exponents, which are displayed in Fig. 4. However, the small 130-MeV exponent may not be as reliable as the others. It is based on fewer data points with poorer statistics than exponents at

TABLE IV. Simultaneous fits of the A dependence at all energies.

Type	Form	χ^2	Exponent
Nonanalog	A^{-x}	2.30	-1.35 ± 0.06
	$(N-Z)(N-Z-1)A^{-x}$	15.9	-3.25 ± 0.13
	$(N)(N-1)A^{-x}$	2.48	-3.51 ± 0.06
DIAS	A^{-x}	7.48	-1.79 ± 0.07
	$(N-Z)(N-Z-1)A^{-x}$	3.15	-3.29 ± 0.04
	$(N)(N-1)A^{-x}$	7.03	-3.72 ± 0.07

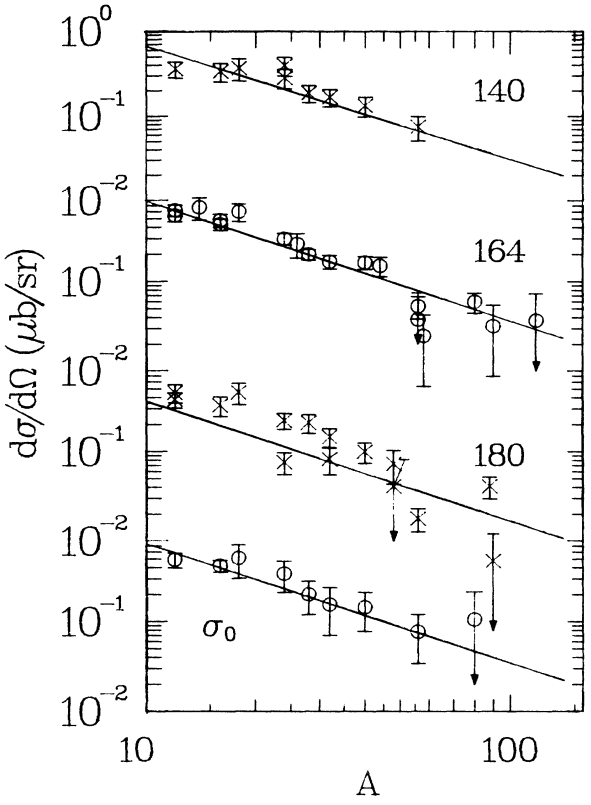

FIG. 3. The mass dependence of nonanalog DCX. Each data set is for constant lab energy, except for the set labeled σ_0, which is the cross section at energy $T=T_0$ (from the excitation function fits in Table II). The lines ares $A^{-4/3}$ curves.

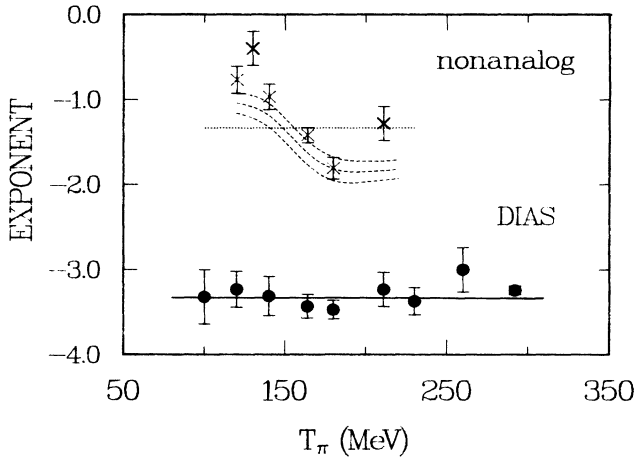

FIG. 4. The variation with energy of the best-fit exponents for the DIAS and nonanalog mass dependences. The DIAS exponents are compared with the expected value of $-\frac{10}{3}$ (solid line). The nonanalog exponents are compared with a prediction (see text) based on the Breit-Wigner excitation-function fits. The dashed lines show the prediction and error bands. The dotted line is at $-\frac{4}{3}$.

TABLE V. Results of nonanalog A^{-x} fits at each energy.[a]

				Constrained $A^{-4/3}$ fit	
T_π	χ^2	f (nb/sr)	Exponent	χ^2	f
120	2.16	93(±12)	−0.77(±0.16)	3.58	60(±6)
130	0.01	154(±28)	−0.40(±0.20)	3.58	59(±12)
140	0.87	133(±16)	−0.97(±0.15)	1.37	105(±9)
164	1.38	118(±8)	−1.42(±0.09)	1.36	124(±6)
180	3.15	50(±5)	−1.81(±0.13)	3.98	56(±5)
210	1.01	53(±9)	−1.28(±0.20)	0.91	51(±4)
$\sigma(T_0)$	0.30	142(±29)	−1.11(±0.22)	1.19	117(±12)
g	1.29	0.025(±0.005)	−1.47(±0.20)	0.38	0.028±(0.003)

[a] $d\sigma/d\Omega(A)=f(A/A_0)^{-x}$, with $A_0=40$.

other energies (see Table III).

We have indicated previously that the shape of nonanalog excitation functions appears to have some mass dependence—in particular, the peak energy decreases with mass (see Table II). If, for example, the peak cross section (independent of energy) follows a power-law mass dependence, the variation of peak energy with mass will result in an energy dependence to the best-fit exponents. For example, at an energy below the peak, an increase in mass effectively moves the excitation function down in energy, increasing the cross section and slowing the mass dependence. At energies above the peak, the cross sections will decrease faster. We have estimated the magnitude of this effect and displayed the result (with error band) as a set of dashed lines in Fig. 4. The variation with energy is similar to that of the best-fit exponents. Thus, we believe that this simple effect accounts for much of the energy variation of the exponents. Given the energy-dependent results, the fits to the energy-independent quantities $\sigma(T_0)$ and g, and the simultaneous fit to all energies, we conclude that, on average, an A dependence of $A^{-4/3}$ represents nonanalog DCX adequately.

Fits to DIAS DCX with the various mass dependences are also shown in Table IV. The only possibly adequate representation of the DIAS mass dependence is the expected mass dependence formula, for which the exponent agrees with the expected value of $-\frac{10}{3}$. The large χ^2 is to be expected; we have already described the variation in the excitation function behaviors at the lower energies. Table VI presents fits with the expected mass dependence formula at each energy. At every energy, the best-fit exponent is consistent with $-\frac{10}{3}$ within errors. (The exponents are also displayed in Fig. 4.) The major energy dependence is the larger χ^2 at the lower energies that result from the greater scatter in the data.

TABLE VI. Results of DIAS $(N-Z)(N-Z-1)A^{-x}$ fits at each energy.[a]

T_π	χ^2	f (nb/sr)	Exponent
100	7.9	12(±4)	−3.32(±0.32)
120	6.4	24(±5)	−3.23(±0.21)
140	6.7	16(±4)	−3.31(±0.23)
164	4.0	15(±2)	−3.43(±0.14)
180	3.4	18(±1)	−3.47(±0.11)
211	0.03	29(±4)	−3.23(±0.20)
230/235	2.8	39(±4)	−3.37(±0.16)
260	1.8	64(±13)	−3.00(±0.26)
292	2.1	68(±3)	−3.24(±0.05)

[a] $d\sigma/d\Omega(A)=f(N-Z)(N-Z-1)(A/A_0)^{-x}$, with $A_0=42$.

IV. DISCUSSION

How are these results to be interpreted? Some important points should be stressed. First, the mass dependences of both analog and nonanalog DCX are reasonably well represented by simple functions over a wide range of masses and energies. In particular, for DIAS DCX, the derivation of the expected mass dependence ignores, for example, nuclear structure (shell effects), alternative reaction mechanisms, intermediate states other than the single-isobaric-analog state, and two-nucleon (or ρ^2) effects. For example, an estimate by Johnson and Siciliano[11] of certain ρ^2 effects indicated that the conventional mass dependence formula would be (approximately) modified by an additional factor of $(N-Z)^2/(N-Z-1)^2$. (This modification does not, however, significantly improve fits at energies where the conventional formula works poorly). Although we have previously emphasized that the χ^2 are large, it is probably more nearly correct to believe that the χ^2 are surprisingly good, given the simple assumptions made.

Second, the mass dependences for analog and nonanalog DCX are dramatically different. For nonanalog DCX, it has been speculated[2,8] that the regular angle, energy, and mass dependences imply dominance by a single, diffractive reaction process. Given the different angle, energy and mass dependences of nonanalog and analog DCX, it is an obvious speculation that the dominant underlying reaction mechanisms for nonanalog and DIAS DCX are different. This is supported by some theoretical results. DIAS DCX is generally assumed to result from sequential charge exchange, with important corrections at and below resonance.[1,2] Calculations of nonanalog DCX through the sequential mechanism result in the same energy dependence as for DIAS DCX,[7,13] and, as there would

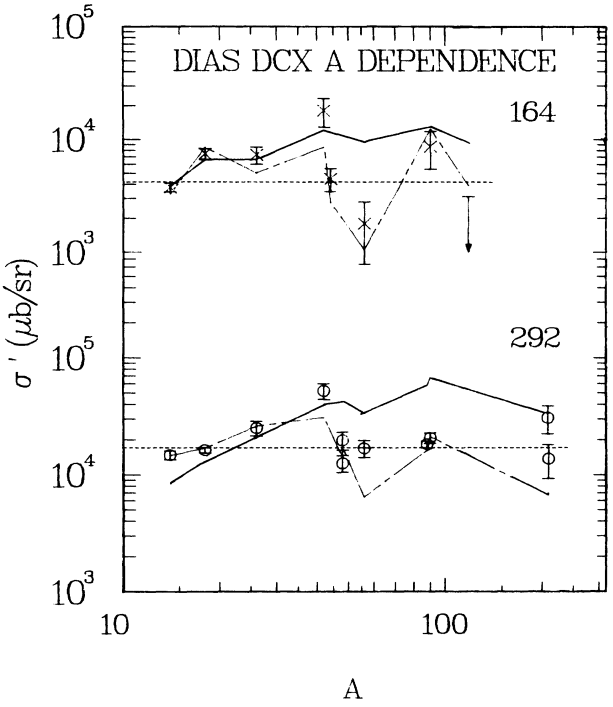

FIG. 5. The mass dependence of DIAS DCX contrasted with a smooth $A^{-10/3}$ mass dependence (dashed line), with lowest-order DCX calculations (jagged solid line), and with higher-order calculations (jagged, long-short—dashed line). Plotted is $\sigma' = d\sigma/d\Omega \times A^{10/3}/(N-Z)(N-Z-1)$.

be no dominant intermediate (analog) state, magnitudes of cross sections would presumably be very sensitive to shell-model effects, and would vary irregularly near closed shells.

The observed nonanalog $A^{-4/3}$ dependence has been interpreted as evidence for a single-step process leading to Δ components of the residual nuclear wave function[14] with $A^{2/3} \times (1/A) = A^{-4/3}$. An alternate interpretation is evidence for a collective enhancement of the cross sections, with $A^{2/3} \times (1/A)^4 \times A^2 = A^{-4/3}$. If nonanalog DCX were sensitive to all neutrons in the nucleus (as discussed above), we would expect a factor of $N(N-1)$ in the mass dependence which, for the existing data set, is equivalent to A^2. This seems consistent with the model of Ref. 7, for which an $A^{-4/3}$ mass dependence for the calculations arises out of the collectivity of the ground state to ground state nuclear matrix elements.

Figure 5 shows the mass dependence of DIAS DCX at 164 and 292 MeV contrasted with the best-fit $A^{-10/3}$ curves, with lowest-order DCX calculations [calculated with the code PIESDEX (Ref. 11) and Skyrme III excess neutron densities for all nuclei], and with higher-order DCX calculations from Ref. 15. At both energies the simple mass dependence formula appears to represent the data about as well as the actual lowest-order calculations (which, it should be noted, do not follow the simple formula and have a slightly different mass dependence at the two energies).

The higher-order optical-potential[15] calculations of Fig. 5 have been used to explain the forward minima exhibited by 164-MeV DIAS angular distributions. For the $T=1$ nuclei (which have been more studied that other nuclei), these ρ^2 terms approximately cancel at 0°, thus leaving the mass dependence mostly unaffected, but interfere at larger angles to produce the forward minima. The higher-order calculations of Fig. 5 at 164 MeV are taken from Ref. 15; the 292-MeV calculations result from an extension of that model to an additional energy. At both energies, the calculated cross sections on heavier nuclei are usually decreased significantly. We note that similar results have been obtained in higher-order calculations by Liu[16,17] for light $T=1$ nuclei and for ^{48}Ca.

In Ref. 6 it was noted that the examination of only $T=1$ nuclei indicates $A^{-7/3}$ mass dependence. No explanation was suggested. The best-fit exponent for a fit to the ^{14}C, ^{18}O, ^{26}Mg, and ^{42}Ca data at 164, 180, 230/235, and 292 MeV is -2.33 ± 0.14 with a χ^2 of 1.9. In view of the $A^{-4/3}$ mass dependence of nonanalog DCX, one could speculate[19] that the interference of the two mechanisms with an $(N-Z)(N-Z-1)A^{-10/3}$ and an $A^{-4/3}$ mass dependence results in the intermediate mass dependence. An examination of the calculations in Fig. 5, however, shows a similarly slower mass dependence for the $T=1$ nuclei. This result occurs because the Skyrme III densities do not scale according to the simple assumption

$$\frac{\Delta\rho}{\rho} = \frac{N-Z}{A} .$$

Instead, $\Delta\rho/\rho$ increases with mass faster than $(N-Z)/A$. Thus, it appears that the $T=1$ mass dependence may arise simply from the excess neutron densities (if this aspect of nuclear structure is correctly represented by the Skyrme densities), rather than from additional reaction mechanisms or higher-order effects.

V. SUMMARY

We have reported the measurement of several new cross sections, and performed an analysis of the mass dependences of the entire available DCX data set. We have quantitatively confirmed that the mass dependence of both analog and nonanalog DCX may be approximated by relatively simple formulas, $(N-Z)(N-Z-1)A^{-10/3}$ for DIAS DCX and $A^{-4/3}$ for nonanalog DCX, that are applicable over a wide range of masses and energies. In both cases, the quality of the agreement between data and formula varies with energy. For DIAS DCX, the mass dependence exponent is independent of energy, but the quality of the agreement is worse at lower energies. For nonanalog DCX, the quality of the agreement is fairly good at each energy, but the exponent varies with energy.

The very different mass, angle, and energy dependences lead to the speculation that there are different underlying reaction mechanisms dominating analog and nonanalog DCX. DIAS DCX is dominated by sequential single-

charge exchange (with important corrections at and below resonance energies) and is sensitive to excess neutron pairs, particularly at the higher energies. Some of the features of the mass dependence are reproduced by the use of microscopic calculations. Some nonsequential mechanism presumably dominates nonanalog DCX, but the proof of this requires, of course, adequate microscopic calculations.

This work was supported by the National Science Foundation, the Robert A. Welch Foundation, and the U. S. Department of Energy.

---

*Present address: Argonne National Laboratory, Argonne, IL 60439.

†Present address: Los Alamos National Laboratory, Los Alamos, NM 87545.

‡Present address: Lawrence Berkeley Laboratory, Berkeley, CA 94720.

§Present address: Indiana University Cyclotron Facility, Bloomington, IN 47405.

**Present address: Kirtland Air Force Base, NM 87117.

††Permanent address: Ben-Gurion University of the Negev, Beer-Sheva, Israel.

‡‡Present address: New Mexico State University, Las Cruces, NM 88003.

[1]Mikkel B. Johnson, Phys. Rev. C **22**, 192 (1980).

[2]C. L. Morris *et al*, Phys. Rev. C **25**, 3218 (1982).

[3]S. J. Greene *et al.*, Phys. Rev. C **25**, 927 (1982).

[4]Peter A. Seidl *et al.*, Phys. Rev. Lett. **50**, 1106 (1983).

[5]K. K. Seth *et al.*, Phys. Lett. **155B**, 339 (1985).

[6]Peter A. Seidl *et al.*, Phys. Rev. C **30**, 973 (1984).

[7]R. Gilman *et al.*, Phys. Rev. C **32**, 349 (1985); **34**, 1895 (1986); A. Wirzba *et al.* (unpublished). See also Mikkel B. Johnson *et al.*, Phys. Rev. Lett. **52**, 593 (1984).

[8]L. C. Bland *et al.*, Phys. Lett. **128B**, 157 (1983).

[9]S. J. Greene *et al.*, Phys. Rev. C **27**, 2375 (1983); R. Gilman *et al.*, *ibid.* **29**, 2395 (1984); **30**, 962 (1984).

[10]F. James and M. Roos, Comput. Phys. Commun. **10**, 343 (1975).

[11]Mikkel B. Johnson and E. R. Siciliano, Phys. Rev. C **27**, 1647 (1983).

[12]See, e.g., various theoretical talks in Proceedings of the LAMPF Workshop on Pion Double Charge Exchange, Los Alamos National Laboratory Report LA-10550-C, 1985.

[13]Consistent calculations of nonanalog and analog DCX have been performed by, e.g., Guang-Lie Li, Chu-Hsia Li, and T.-S. H. Lee, Phys. Lett. **99B**, 200 (1981). Liu Xianhui, Wu Zongen, Huang Zhaohui, and Li Yangguo, Sci. Sin. **24**, 784 (1981); T. Karapiperis and M. Kobayashi, SIN Report PR-84-14, 1984.

[14]L. C. Bland *et al.*, J. Phys. G **8**, L173 (1982).

[15]Steven J. Greene *et al.*, Phys. Rev. C **30**, 2003 (1984).

[16]L. C. Liu, Phys. Rev. C **27**, 1611 (1983).

[17]Kamal K. Seth *et al.*, Phys. Rev. Lett. **52**, 894 (1984).

[18]Other data is from C. L. Mooris *et al.*, Phys. Rev. Lett. **45**, 1233 (1980); **54**, 775 (1985); Steven J. Greene *et al*, Phys. Lett. **88B**, 62 (1979); H. Nann *et al.*, *ibid.* **96B**, 261 (1980); R. Gilman *et al.*, Phys. Rev. C **30**, 958 (1984); Peter A. Seidl *et al.*, Phys. Lett. **154B**, 339 (1985); Mark. O. Kaletka, Ph.D. thesis, Northwestern University, 1983, available as Los Alamos National Laboratory thesis report LA-9947-T, 1984.

[19]H. T. Fortune and R. Gilman, Phys. Rev. C **33**, 2171 (1986).